Predicting Temperature Increase through Local SAR Estimation by B1 Mapping: A Phantom Validation at 7T

Xiaotong Zhang, *Member, IEEE,* Jiaen Liu, *Student Member, IEEE,* Sebastian Schmitter, Pierre-Francois Van de Moortele, and Bin He, *Fellow, IEEE*

Abstract— **It has been shown that Electrical Properties d(EPs) of biological tissues can be derived from MR-based B1 measurement. A strong appeal for these 'Electrical Property Tomography' (EPT) methods is to estimate real-time and subject-specific local specific absorption rate (SAR) induced by RF transmission. In order to investigate the feasibility of EPT-based local SAR estimation, following previously proposed EPT protocols, induced local SAR has been firstly estimated under one B1 shim setting for a heating sequence at 7T; whereas with the same acquired B1 information, induced local SAR under a different B1 shim setting has been further predicted. Both of the SAR results have been compared to measured temperature changes using MRI Thermometry based on the proton chemical shift.**

I. Introduction

Ultra-high-field (UHF) Magnetic Resonance Imaging (MRI) systems (operating at 7 Telsa or higher magnetic fields) have been pursued with increasing interest [1]. Their main advantages include higher signal-to-noise ratio (SNR) enabling higher spatial and/or temporal resolution, and increased sensitivity for intrinsic contrast mechanisms such as blood oxygenation level-dependent (BOLD) contrast. However, the magnitude of electric fields generated for a given strength of the transmit magnetic field increases with the operating radio frequency (RF) (approximately proportional to the main magnetic field strength); the electric fields induce eddy currents and hence dissipate heat into the human body, resulting in elevated energy deposition as the frequency increases [2]. Possible local overheating poses a serious safety concern at UHF.

To limit the in-vivo temperature rise, current guidelines (International Standard IEC 60601-2-33 2010) impose upper limits on global specific absorption rate (SAR) as well as on peak local SAR averaged through 10 gram of tissue. In practice, at UHF local averaged SAR often reaches maximum upper limits before global SAR at UHF [3]. The estimation of local SAR for human MR experiments typically relies on time-consuming computational electromagnetic simulations. Such extensive computations have been conducted using a variety of commercial software, based on the numerical models of EM properties of the human body [4][5]. However, beside the time-consuming constraint of these simulation approaches, it remains to be shown whether such findings based on a very limited number of different individuals' anatomy could reliably provide a quantitative prediction of local SAR characteristics of a given specific subject undergoing a scan. As such, real-time and subject-specific local SAR estimation is highly desired in UHF MRI applications.

MR based Electrical Properties Tomography (EPT) utilizes measurable RF-coil-induced magnetic fields (B1 fields) in an MRI system to quantitatively reconstruct the local EPs of biological tissues. Based upon well-established B1-mapping techniques [6]–[11] in MRI, various MR-EPT methods have been proposed using different coil designs (e.g. birdcage quadrature, multi-channel transmit) and at different radio frequencies (64MHz~300MHz) corresponding to different operating static main magnetic fields (1.5T~7T) [12]–[20]. EPT reconstructs EPs at the operating Larmor frequency; knowing EPs distribution can help deduce RF electric fields, allowing for fast, subject-specific SAR estimation and management for the purpose of constraining tissue heating in pulse sequence design in UHF-MRI applications.

In order to investigate the feasibility of EPT-based local SAR estimation in predicting possible local temperature change, following the proposed EPT protocols in [19], [20], in this preliminary study, induced local SAR in a saline phantom has been *estimated* and *predicted* for a heating MRI sequence under two B1 shim settings, respectively. Calculated local SAR were compared to measured temperature changes using MRI Thermometry based on the proton chemical shift (PRF) [21].

II. Methods

A single-compartment cylinder phantom (12cm in radius and 20cm in height), consisting of H2O, NaCl, $Cu_2SO_4 \cdot 5H2O$ and Gelatin (mass ratio 100:0.27:0.1:3), was constructed with

This work was supported in part by NIH EB017069, EB006433, EB007920, EB009133, EB014353, RR008079, NS057091, and HL117664.

X. Zhang is with the Department of Biomedical Engineering, University of Minnesota, Minneapolis, MN 55455, USA.
J. Liu is with the Department of Biomedical Engineering, University of Minnesota, Minneapolis, MN 55455, USA.
S. Schmitter is with the Center for Magnetic Resonance Research, University of Minnesota, Minneapolis, MN 55455, USA.
P.-F. Van de Moortele is with the Center for Magnetic Resonance Research, University of Minnesota, Minneapolis, MN 55455, USA.
B. He is with the Department of Biomedical Engineering and Institute for Engineering in Medicine, University of Minnesota, Minneapolis, MN 55455, USA.

978-1-4244-7929-0/14/$26.00 ©2014 IEEE

conductivity 0.56S/m, permittivity 75.7, mass density 1033kg/m^3 and heat capacity $C_{phantom}$=4.2kJ/kg/K. EPs measurements were conducted with an Agilent 85070D dielectric probe kit and an Agilent E4991A network analyzer at 298MHz. Three mineral oil phantoms were attached to the surface of the phantom, providing a reference for phase drift corrections [22]. The phantom was imaged in a 7T scanner (Siemens) equipped with an elliptical 16-channel head transceiver coil [23] after being placed in the bore overnight to achieve thermal equilibrium. 12 contiguous transverse slices were sampled at a spatial resolution of 1.5×1.5×3mm^3. Two B1 phase shim settings were employed sequentially, approximating two different Circularly Polarized (CP) modes: (I) with stronger B1 in the periphery (CP2+ mode like), and (II) with stronger B1 in the center (standard CP mode-like).

RF-heating was obtained with a simple sequence consisting of a 2ms square RF pulse applied every 200ms for duration of 3min per run, without any encoding gradient. Temperature measurements were performed using the PRF technique [21], based on phase maps acquired with a 3D GRE sequence (TE=10ms, TR=15ms, acquisition time 30s with 1 average and accelerated with GRAPPA2 [24]). These phase maps were obtained before, during (the heating sequence was run consecutively 8 times with one phase measurement between each run), and after (9 phase measurements distributed over 30 min) RF-heating. These phase images were then converted into temperature maps according to [21], [22].

As described in [25], [26], a series of 16 small flip angle GRE images were acquired with each individual channel transmitting at a time while receiving all together; a 3D map of the excitation flip angle was obtained with the AFI technique [7]. Based on these data, transmit B1 magnitude for each coil element, and their relative phase maps between coil elements were calculated. Then the absolute phase of transmit B1 can be calculated voxel-wisely as in [20]. Finally, the voxel-wise

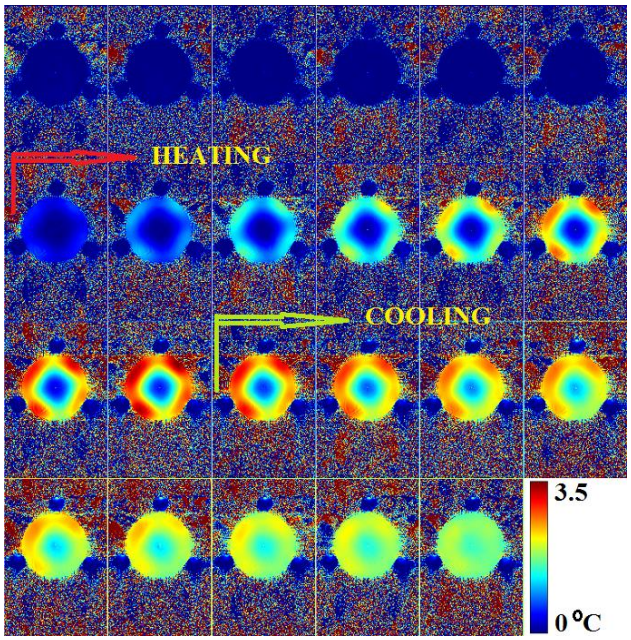

FIG. 1 B1 shim I. Measured Temperature change using MRI Thermometry. The first phase image acquired before heating was taken as

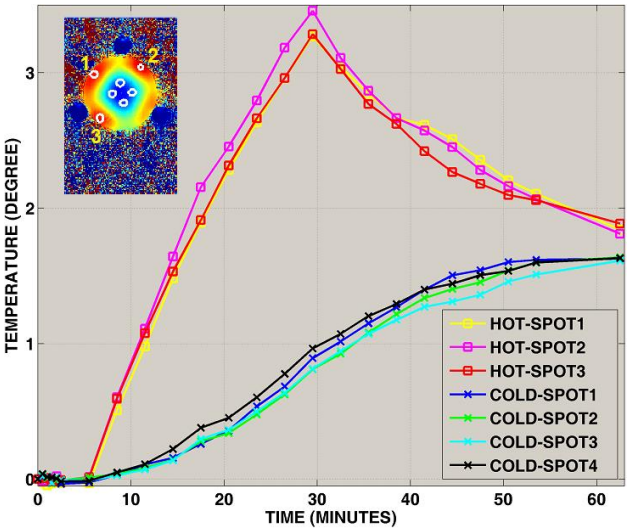

FIG. 2 B1 shim I. Time course of measured temperature change at seven local "hot" and "cold" spots.

local SAR for the shimmed excitation can be estimated using complex transmit B1 and probe-measured EPs under the assumption of a dominant z-component of electric fields compared to other transverse components as described in [15], [19], and averaged into 10-gram SAR.

For a limited period of time (up to several minutes) after starting RF-heating, thermal conduction can be neglected, and the temperature increase ΔT over time can be treated as proportional to the induced local SAR [22]; therefore, local SAR distribution is expected to have a spatial pattern similar to that of ΔT map.

In this study, PRF-based temperature measurements under two B1 shim settings were conducted separately. By employing the proposed EPT approach as in [19], [20], Local SAR under B1 shim setting I was firstly *estimated* based on B1 measurement under shim I, whereas local SAR under shim II was *predicted* based on B1 measurement under shim I and with the knowledge of phase adjustment from shim I to II.

III. Results

Under B1 shim setting I, ΔT maps on slice #6 measured by PRF before, during and after RF-heating are shown in Fig.1. Two dramatically different types of temperature-change time-courses, plotted in Fig.2, were observed when comparing local spots located among the highest ΔT values ("hot spot", in the periphery) with local spots located among the lowest ΔT values ("cold spot", close to the center). Consistent with

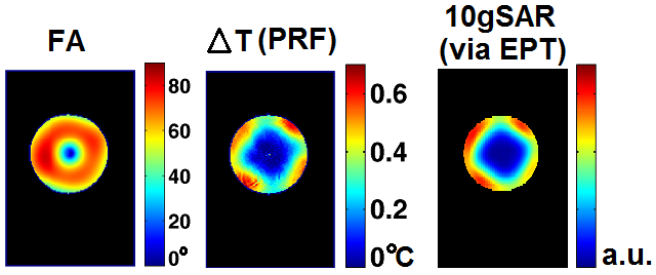

FIG. 3 B1 shim I. Measured actual flip angle (left), measured temperature change by PRF (middle), and estimated local 10gSAR (right).

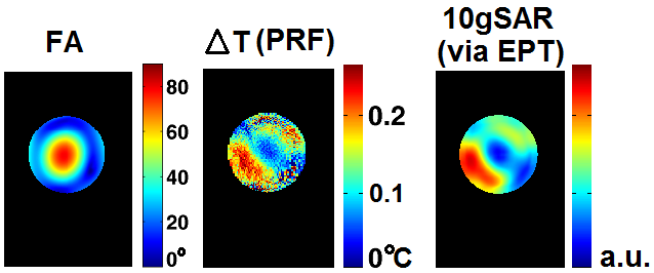

FIG. 4 B1 shim II. Measured actual flip angle (left), measured temperature change by PRF (middle), and *predicted* local 10gSAR

findings in [22], in the hottest spots, where local SAR is expected to be the dominant source of temperature variation, prominent ΔT per unit of time was observed during and after RF-heating with a sharp curve discontinuity in the between; on the contrary, and still consistent with [22], in colder spots (where SAR is expected to be minimal with thermal conduction being the dominant source of temperature variation), the temperature increased at a much slower pace and kept increasing even after RF heating was turned off, slowly tending to reach a plateau within the total duration of the experiment. In order to compare the spatial distribution of *estimated* or *predicted* 10gSAR versus that of temperature increase, only the ΔT measurement obtained after the 1st heating run (3min) was considered in order to minimize thermal conduction contribution (negligible during this period of time).

Under B1 shim setting I, measured flip angle (FA) map, measured ΔT map and *estimated* 10gSAR map (in arbitrary unit) are shown, within the slice of interest (slice #6), in Fig.3. A reasonable similarity can be observed between ΔT and 10gSAR maps, including four regional hot spots relatively symmetrically distributed in the periphery and a diamond-shaped colder center region.

Under B1 shim setting II, FA map, measured ΔT map and predicted 10gSAR map (in arbitrary unit) are shown, within the same slice, in Fig.4. Although an unexpected level of noise observed in the measured ΔT map, which will require further investigation, ΔT and 10gSAR maps exhibit a similar overall spatial pattern.

IV. Discussion and Conclusion

Reasonable agreement has been observed between distributions of MRI Thermometry measurement and estimated SAR via EPT. Future work includes quantitative validation by comparing EPT-based temperature prediction (in real metric unit) and actual measured temperature (e.g. by MRI Thermometry), with the goal of further validating safety limits in the MRI scanner on a per-subject basis.

Acknowledgment

We thank Dr. Xiaoping Wu for technical support.

References

[1]K. Uğurbil, G. Adriany, P. Andersen, W. Chen, M. Garwood, R. Gruetter, P.-G. Henry, S.-G. Kim, H. Lieu, I. Tkac, T. Vaughan, P.-F. Van De Moortele, E. Yacoub, and X.-H. Zhu, "Ultrahigh field magnetic resonance imaging and spectroscopy," *Magn. Reson. Imaging*, vol. 21, no. 10, pp. 1263–1281, Dec. 2003.

[2]T. Vaughan, M. Garwood, C. Collins, W. Liu, L. DelaBarre, G. Adriany, P. Andersen, H. Merkle, R. Goebel, M. Smith, and K. Ugurbil, "7T vs. 4T: RF power, homogeneity, and signal-to-noise comparison in head images," *Magn. Reson. Med.*, vol. 46, no. 1, pp. 24–30, 2001.

[3]D. Shrivastava, T. Hanson, J. Kulesa, J. Tian, G. Adriany, and J. T. Vaughan, "Radiofrequency heating in porcine models with a 'large' 32 cm internal diameter, 7 T (296 MHz) head coil," *Magn. Reson. Med.*, vol. 66, no. 1, pp. 255–263, 2011.

[4]C. M. Collins, W. Liu, J. Wang, R. Gruetter, J. T. Vaughan, K. Ugurbil, and M. B. Smith, "Temperature and SAR calculations for a human head within volume and surface coils at 64 and 300 MHz," *J. Magn. Reson. Imaging JMRI*, vol. 19, no. 5, pp. 650–656, May 2004.

[5]S. Wolf, D. Diehl, M. Gebhardt, J. Mallow, and O. Speck, "SAR simulations for high-field MRI: How much detail, effort, and accuracy is needed?," *Magn. Reson. Med.*, vol. 69, no. 4, pp. 1157–1168, 2013.

[6]E. K. Insko and L. Bolinger, "Mapping of the radiofrequency field," *J. Magn. Reson. A*, vol. 103, no. 1, pp. 82–85, Sep. 2013.

[7]V. L. Yarnykh, "Actual flip-angle imaging in the pulsed steady state: A method for rapid three-dimensional mapping of the transmitted radiofrequency field," *Magn. Reson. Med.*, vol. 57, no. 1, pp. 192–200, Jan. 2007.

[8]G. R. Morrell, "A phase-sensitive method of flip angle mapping," *Magn. Reson. Med.*, vol. 60, no. 4, pp. 889–894, 2008.

[9]L. I. Sacolick, F. Wiesinger, I. Hancu, and M. W. Vogel, "B1 mapping by Bloch-Siegert shift," *Magn. Reson. Med.*, vol. 63, no. 5, pp. 1315–1322, 2010.

[10] G. Helms, J. Finsterbusch, N. Weiskopf, and P. Dechent, "Rapid radiofrequency field mapping in vivo using single-shot STEAM MRI," *Magn. Reson. Med.*, vol. 60, no. 3, pp. 739–743, 2008.

[11] K. Nehrke and P. Börnert, "DREAM—a novel approach for robust, ultrafast, multislice B1 mapping," *Magn. Reson. Med.*, vol. 68, no. 5, pp. 1517–1526, 2012.

[12] E. M. Haacke, L. S. Petropoulos, E. W. Nilges, and D. H. Wu, "Extraction of conductivity and permittivity using magnetic resonance imaging," *Phys. Med. Biol.*, vol. 36, no. 6, pp. 723–734, Jun. 1991.

[13] H. Wen, "Noninvasive quantitative mapping of conductivity and dielectric distributions using RF wave propagation effects in high-field MRI," presented at the Proc. of SPIE, San Diego, CA, USA, 2003, vol. 5030, pp. 471–477.

[14] U. Katscher, T. Voigt, C. Findeklee, P. Vernickel, K. Nehrke, and O. Dossel, "Determination of Electric Conductivity and Local SAR Via B1 Mapping," *Med. Imaging IEEE Trans. On*, vol. 28, no. 9, pp. 1365–1374, Sep. 2009.

[15] T. Voigt, U. Katscher, and O. Doessel, "Quantitative conductivity and permittivity imaging of the human brain using electric properties tomography," *Magn. Reson. Med.*, vol. 66, no. 2, pp. 456–466, 2011.

[16] A. L. van Lier, D. O. Brunner, K. P. Pruessmann, D. W. J. Klomp, P. R. Luijten, J. J. W. Lagendijk, and C. A. T. van den Berg, "B 1+ Phase mapping at 7 T and its application for in vivo electrical conductivity mapping," *Magn. Reson. Med.*, vol. 67, no. 2, pp. 552–561, 2012.

[17] U. Katscher, C. Findeklee, and T. Voigt, "B1-based specific energy absorption rate determination for nonquadrature radiofrequency excitation," *Magn. Reson. Med.*, vol. 68, no. 6, pp. 1911–1918, 2012.

[18] X. Zhang, P.-F. V. de Moortele, S. Schmitter, and B. He, "Complex B1 mapping and electrical properties imaging of the human brain using a 16-channel transceiver coil at 7T," *Magn. Reson. Med.*, vol. 69, no. 5, pp. 1285–1296, 2013.

[19] X. Zhang, S. Schmitter, P. Van de Moortele, J. Liu, and B. He, "From Complex B1 Mapping to Local SAR Estimation for Human Brain MR Imaging Using Multi-Channel Transceiver Coil at 7T," *IEEE Trans. Med. Imaging*, vol. 32, no. 6, pp. 1058–1067, 2013.

[20] J. Liu, X. Zhang, P.-F. Van de Moortele, S. Schmitter, and B. He, "Determining electrical properties based on B(1) fields measured in an MR scanner using a multi-channel transmit/receive coil: a general approach," *Phys. Med. Biol.*, vol. 58, no. 13, pp. 4395–4408, Jul. 2013.

[21] Y. Ishihara, A. Calderon, H. Watanabe, K. Okamoto, Y. Suzuki, K. Kuroda, and Y. Suzuki, "A precise and fast temperature mapping using water proton chemical shift," *Magn. Reson. Med.*, vol. 34, no. 6, pp. 814–823, 1995.

[22] S. Oh, A. G. Webb, T. Neuberger, B. Park, and C. M. Collins, "Experimental and numerical assessment of MRI-induced temperature change and SAR distributions in phantoms and in vivo," *Magn. Reson. Med.*, vol. 63, no. 1, pp. 218–223, Jan. 2010.
[23] G. Adriany, P.-F. Van de Moortele, J. Ritter, S. Moeller, E. J. Auerbach, C. Akgün, C. J. Snyder, T. Vaughan, and K. Uğurbil, "A geometrically adjustable 16-channel transmit/receive transmission line array for improved RF efficiency and parallel imaging performance at 7 Tesla," *Magn. Reson. Med.*, vol. 59, no. 3, pp. 590–597, Mar. 2008.
[24] M. A. Griswold, P. M. Jakob, R. M. Heidemann, M. Nittka, V. Jellus, J. Wang, B. Kiefer, and A. Haase, "Generalized autocalibrating partially parallel acquisitions (GRAPPA)," *Magn. Reson. Med.*, vol. 47, no. 6, pp. 1202–1210, 2002.
[25] P.-F. Van de Moortele, C. Akgun, G. Adriany, S. Moeller, J. Ritter, C. M. Collins, M. B. Smith, J. T. Vaughan, and K. Uğurbil, "B1 destructive interferences and spatial phase patterns at 7 T with a head transceiver array coil," *Magn. Reson. Med.*, vol. 54, no. 6, pp. 1503–1518, Dec. 2005.
[26] P.-F. Van de Moortele, C. Snyder, L. DelaBarre, G. Adriany, J. T. Vaughan, and K. Ugurbil, "Calibration Tools for RF Shim at Very High Field with Multiple Element RF Coils: from Ultra Fast Local Relative Phase to Absolute Magnitude B1+ Mapping," presented at the Proc. of ISMRM, Berlin, Germany, 2007, p. 1676.